Environment and Ecology 37 (1B) : 333—343, January—March 2019
Website: environmentandecology.com ISSN 0970-0420

NDWI Differencing and Post-Classification to Detect Water Body Changes in Karun Basin, Iran

Sajjad Shakerian, Hassan Torabi Podeh, Hamed Naghavi, Babak Shahinejad

Received 10 October 2018 ; Accepted 15 November 2018 ; Published on 6 December 2018

Abstract In recent years the rainfall in Iran have been reduce. Although the Iranian Government try to reduce undesirable effects of rainfall reduction by some water construction. His study presents water body change detecting in Karun basin and we try to evaluate change of water content in the most important basin in Iran (Karun basin) by using remote sensing method. The Normalized Difference Water Index (NDWI) image differencing and post-classification techniques were applied to calculate the change of water content since of 1992 by Landsat-5 (TM) images to 2017 by Landsat-8 (OLI) images the NDWI was derived first then classified to produce vegetation and water body maps followed by quantifying the changes. The results indicated an intense decrease in the sparse vegetation and slight water bodies by 4302 km^2 (6.4%), 593 km^2 (0.9%) respectively. In contrast, the highest increase occurring in no vegetation class (other land cover) of 3664 km^2 (5.4%).

Keywords Water body changes, NDWI image differencing, Landsat-5 (TM), Landsat-8 (OLI), Post-classification.

Sajjad Shakerian*
PhD Student Hydraulic Structures, Faculty of Agriculture, University of Khoramabad, Lorestan, Iran

Hassan Torabi Podeh
Associated Professor of Department of Agriculture, University of Khoramabad, Lorestan, Iran

Hamed Naghavi
Associated Professor of Department of Forestry, Faculty of Agriculture and Natural Resources, University of Khoramabad, Lorestan, Iran

Babak Shahinejad
Associated Professor of Department of Agriculture, University of Khoramabad, Lorestan, Iran
e-mail:shakeriansajjad@gmail.com
*Corresponding author

Introduction

Remote sensing imaging is considered one of the main sources of information about the Earths cover. They have been widely used in detecting and monitoring land cover changes at various scales because of the capability of remote sensing technology to provide a broad range of calibrated, objective, repeatable and cost-effective data for large and regional areas (Campbell 2002, Richards and Jia 2006 and Richards 2012). Furthermore, they have been found suitable for a wide range of applications. Among remote sensing applications is detecting water and moisture content changes.

As an important part of the Earths water cycle, land surface water bodies, such as rivers, lakes and reservoirs, are irreplaceable for the global ecosystem and climate system. Surveying land surface water bodies and delineating their spatial distribution has a great significance to understanding hydrology processes and managing water resources (Papa et al. 2008, Vorosmarty et al.1997). At present, remote sensing has become a routine approach for land surface water bodies monitoring, because the acquired data can provide macroscopic, real-time, dynamic and cost-effective information, which is substantially different from conventional *in situ* measurements

(Chen et al. 2004, Feng et al. 2012). Various methods, including single band density slicing (Work and Gilmer 1976), unsupervised and supervised classification (Huang et al. 2014, Du et al. 2014) and spectral water indexes (Li et al. 2016), were developed in order to extract water bodies from different remote sensing images.

Among all existing water body mapping methods, the spectral water index-based method is a type of reliable method, because it is user friendly, efficient and has low computational cost (Ryu et al. 2002, Sivanpillai and Miller 2010). Different water indexes have already been proposed in the past few decades. Specifically, McFeeters (1996) proposed the Normalized Difference Water Index (NDWI) (McFeeters 1996), using the green and Near Infrared (NIR) bands of remote sensing images based on the phenomenon that the water body has strong absorbability and low radiation in the range from visible to infrared wavelengths. NDWI can enhance the water information effectively in most cases, but it is sensitive to built-up land and often results in over-estimated water bodies. Many previous research works have demonstrated that MNDWI is more suitable to enhance water information and can extract water bodies with greater accuracy than NDWI (Du et al. 2014, Li et al. 2013, Xu 2006, Singh et al. 2015). For regional studies, images provided by the Thematic Mapper (TM) and the latest Operational Land Imager (OLI) from Landsat series satellites are popular datasets. For example, Hui et al. (2008) modelled the spatial and temporal change of Poyang Lake using multi-temporal Landsat TM and ETM + images (Hui et al. 2008). Du et al. (2014) extracted the water body maps at subareas over the Yangtze River Basin and Huaihe River Basin in China from Landsat OLI images (Du et al. 2014). Rokni et al. (2014) extracted water features and detected change using Landsat TM, ETM + and OLI images (Rokni et al. 2014). Compared to MODIS, the Landsat TM, ETM + and OLI images have much finer spatial resolutions (30 m) and can extract open water bodies with more explicit and accurate boundaries.

The post-classification method is widely used to quantify changes. This method involves comparative analysis of independent spectral classifications of images acquired on two different dates. It is characterized by easy calculation and provides from-to change information. It also has equal capability of mapping the kind of landscape transformation that has occurred between the 2 dates under consideration. It is worth mentioning , however, that the overall accuracy of the product depends on the accuracy of the individual classification (Al-doski et al. 2013). During drought event, vegetation canopy can be affected by water stress. This can have major impact on the plant development in general and can cause crop failure or lower crop production in agricultural areas. Early recognition of plant water stress can be critical to prevent such consequences. By providing near-real time information on the plant water stress to the stakeholders, water and agricultural management can be much improved, notably by irrigating specifically areas where plant water needs are not fulfilled anymore.

The Normalized Difference Water Index (NDWI) is known to be strongly related to the plant water content. It is therefore a very good proxy for plant water stress. The Normalized Difference Water Index (NDWI) (Gao 1996) is a satellite-derived index from the Near Infrared (NIR) and Short Wave Infrared (SWIR) channels. The SWIR reflectance reflects changes in both the vegetation water content and the spongy mesophyll structure in vegetation canopies, while the NIR reflectance is affected by leaf internal structure and leaf dry matter content but not by water content. The combination of the NIR with the SWIR removes variations induced by leaf internal structure and leaf dry matter content, improving the accuracy in retrieving the vegetation water content (Ceccato et al. 2001). The amount of water available in the internal leaf structure largely controls the spectral reflectance in the SWIR interval of the electromagnetic spectrum. SWIR reflectance is therefore negatively related to leaf water content (Tucker 1980). Its usefulness for drought monitoring and early warming has been demonstrated in different studies (Ceccato et al. 2002, Gu et al. 2007). It is computed using the Near Infrared (NIR) and the Short Wave Infrared (SWIR) reflectance, which makes it sensitive to changes in liquid water content and in spongy mesophyll of

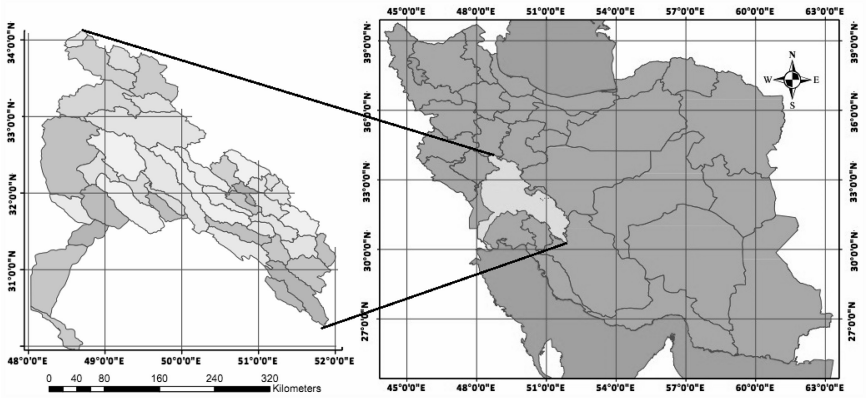

Fig. 1. Iran and the case study area (Karun basin).

vegetation canopies (Ceccato et al. 2002).
Study area and data description

Description of study area

The great basin of Karun in the Zagros highlands is the most important basin in the southwest part of Iran. The great Karun basin consists of the Dez and Karun rivers in the Zagros highlands. The largest river by discharge in Iran, the Karun river is around 950 kilometers (590 mi) long and has an average discharge of 575 cubic meters per second (20,300 cu ft/s). Water from the Karun provides irrigation to over 280,000 hectares (690,000 acres) of the surrounding plain and a further 100,000 hectares (250,000 acres) are planned to receive water (Khuzestan Water and Power Authority 2010). This basin is limited to geographical coordinates 29°58′ to 34°06′ degrees north latitude and 51°57′ to 48°00′ degrees east longitude. The basin area is 67,257 square kilometers, 67% of it is in mountainous areas and plains are form its 33% of area.

The highest point in this region is the Dena with the height of 4409 meters and its lowest point is located in Shalou Bridge with the height of 700 meters. This range consists of 43 main sub-basins (Fig. 1).

Landsat satellite imagery

The Operational Land Imager (OLI) on-board the

Table 1. Comparison between Landsat-8/OLI and Landsat-5/TM (L8).

	Landsat-8/OLI				Landsat-5/TM		
	Band	Wavelength (μm)	Resolution (m)	Band		Wavelength (μm)	Resolution (m)
1	Ultra Blue	0.435–0.451	30	1	Blue	0.45–0.52	30
2	Blue	0.452–0.512	30	2	Green	0.52–0.60	30
3	Green	0.533–0.590	30	3	Red	0.63–0.69	30
4	Red	0.636–0.673	30	4	(NIR)	0.76–0.90	30
5	(NIR)	0.851–0.879	30	5	(SWIR) 1	1.55–1.75	30
6	(SWIR) 1	1.566–1.651	30	6	Thermal	10.40–12.50	120
7	(SWIR) 2	2.107–2.294	30	7	(SWIR) 2	2.08–2.35	30
8	Panchromatic	0.503–0.676	15	–		–	–
9	Cirrus	1.363–1.384	30	–		–	–
10	(TIRS) 1	10.60–11.19	100	–		–	–
11	(TIRS) 2	11.50–12.51	100	–		–	–

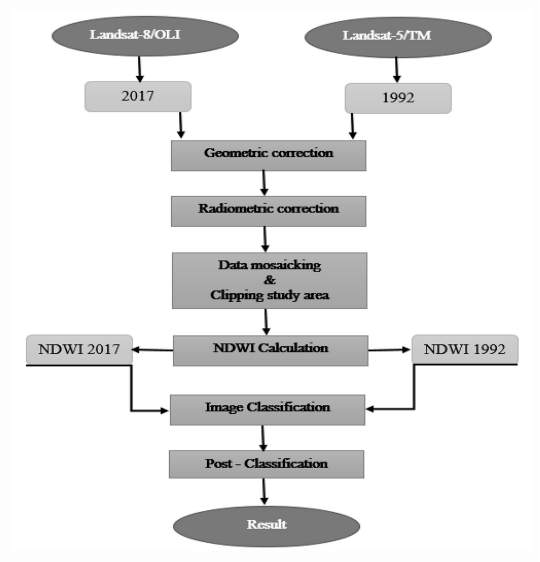

Fig. 2. Flow diagram of methodology.

Landsat-8 was launched by the National Aeronautics and Space Administration (NASA) and the United States Geological Survey (USGS 2015) on 17 February 2013 from the Vandenberg Air Force Base in California. The Landsat-8/OLI offers significant improvements in both the data quality and spectral coverage compared with the Landsat-TM/ETM+and has obtained a large number of clear images so far. Since the launch of Landsat 1 in 1972, the imagery from the Landsat series of satellites has become the longest continuous dataset of reasonable high spatial-resolution imagery for Earth observing, which is widely used for many types of remote sensing applications, such as land surface parameter retrieval, land use and land cover change (Zhong et al. 2014, Thorne et al. 1997) and cross-calibration for other sensors (Hu et al. 2001, Thome et al. 2003). The Landsat-8 was launched to continue Landsat's mission of monitoring Earth systems and capturing changes at a relatively high spatial resolution (Pahlevan et al. 2014, Markham et al. 2015). In addition to fulfilling the Landsat goal in data continuity, the Landsat-8 offers significant improvements in both data quality and spectral coverage (Markham et al. 2015). The Landsat-8 has an Operational Land Imager, which is abbreviated as OLI (hereafter, the OLI sensor on -board the Landsat-8 satellite is written as Landsat-8 / OLI) and a Thermal Infrared Sensor on-board. The Ball Aerospace and Technology Corporation designed the OLI sensor and it includes 9 bands covering the visible, near infrared and short wave infrared portions of the spectrum (Markham et al. 2012). The OLI has spatial and spectral characteristics similar to those of the Thematic Mapper (TM) and Enhanced Thematic Mapper Plus (ETM+), but it also includes some enhancements. The comparison of the band settings, spectral range and spatial resolution between OLI and TM is listed in Table 1.

It is possible to choose image Landsat-7 (ETM+) or Landsat-8 (OLI) for 2017. The OLI is chosen as the reference sensor for the following reasons replace ETM+: The OLI imagery is more quality than the ETM+. Because the airborne scan line corrector in Landsat-7 (ETM+) failed for some reason on 31 May 2003, the collected images have missed some stripes (Tollefson 2013), this has seriously affected the application of Landsat. Instead, at least 400 scenes are collected by OLI daily ; these data become available for downloading within 24 h of acquisition.

Subsequently, the higher radiometric performance, the higher number of bits of radiometric quantization and the easy access of the Landsat-8/ OLI make it a better reference sensor than the ETM+ (Yang et al. 2015). Landsat-5 is still operating with on-board Thematic Mapper (TM) sensor that include 30 m visible and several additional bands in the Short Wave Infrared (SWIR) and thermal-IR band with a spatial resolution of 120 m (Anonymous 2012).

Thirty cloud-free Landsat-5 (TM) images acquired on 1992 and 12 cloud-free Landsat-8 (OLI) on 2017 over a 26 year period within path 163–166, row 36–39 covering the northeast of Iran were obtained. The images are available for free at the Global Land Cover website (http://glcf.umiacs.umd.edu).

Materials and Methods

The overall methodology of this study is briefly presented below:

Pre-processing

Before using data for detecting water body changes,

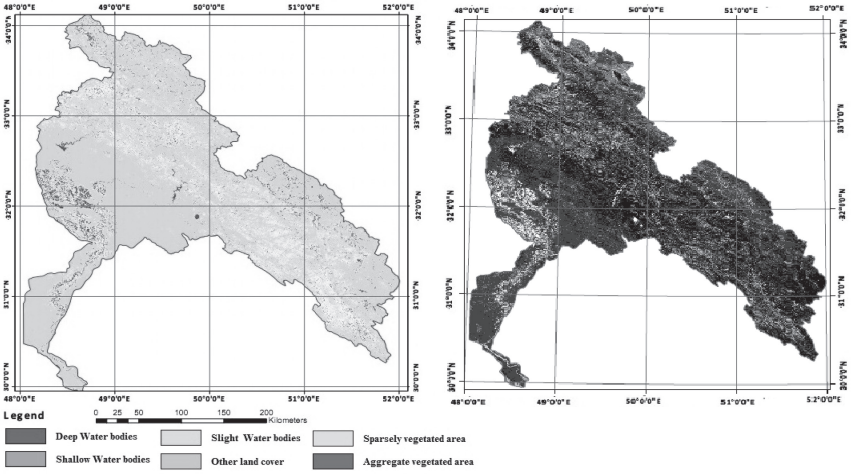

Fig. 3. NDWI images and reclassified image from 1992.

a series of pre-processing operations were performed on 2 images including geometric and radiometric corrections.

Geometric correction of satellite images involves modeling the relationship between the image and ground coordinate systems. All 1992 and 2017 images were rectified to a common Universal Transverse Mercator (UTM) WSG84 Datum, 39 zone coordinate system and registered using image to image method on a November 2014 Landsat OLI image.

A second order polynomial transformation and using a nearest neighbor algorithm for resampling was performed on their respective spatial resolutions. The transformation had a root mean square (RMS) error of 0.4 and 0.38 for 1992 and 2017 images respectively, indicating that the images were accurate to within one pixel (Papa et al. 2008).

Radiometric correction of remotely sensed data is normally carried out to reduce the influence of inconsistencies that may affect the ability to quantitatively analyze as well as interpret images (Paolini et al. 2006). Due to the lack of coexisting reference data

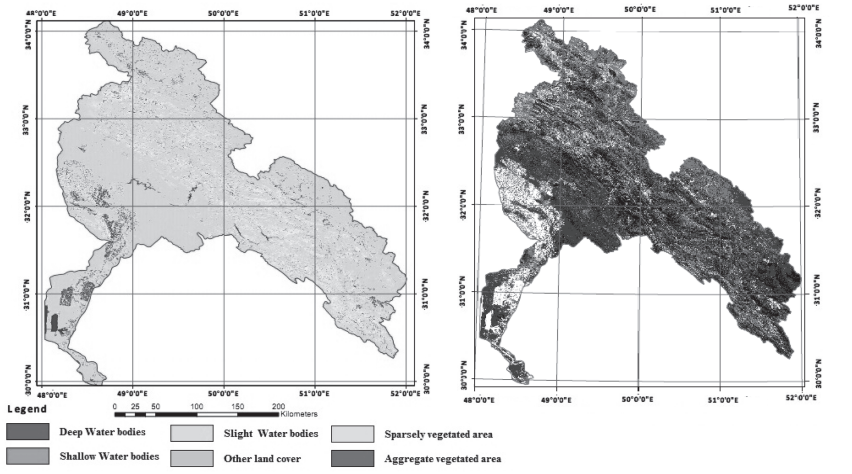

Fig. 4. NDWI images and reclassified image from 2017.

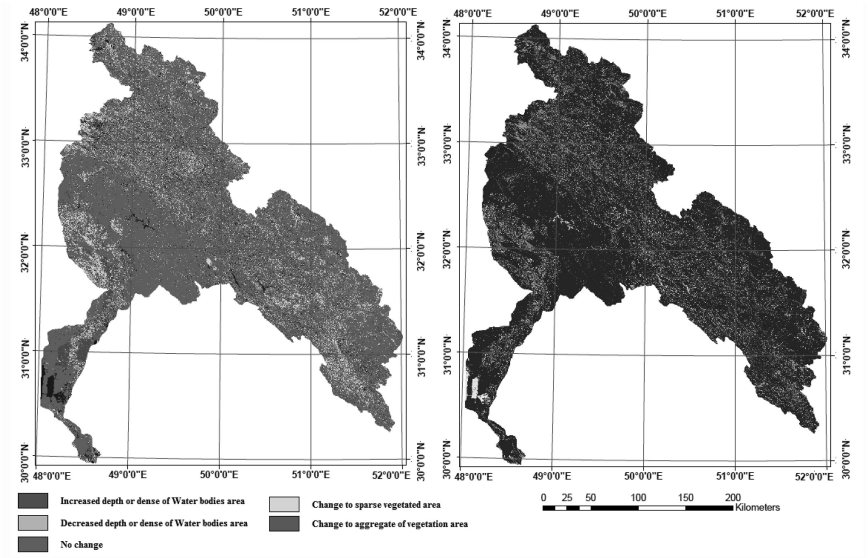

Fig. 5. DNDWI images and reclassified image from change land cover between 1992-2017.

about these images, the relative radiometric correction method was applied to overcome this difficulty.

This method involved two steps: Firstly, converting digital numbers (DNs) to at-satellite spectral radiance by using standard calibration then converting radiance to reflectance values to remove temporal differences in sensor calibration and in environmental factors images. The images were taken from different environment condition and different satellite sensor (OLI/TM), thus, the atmospheric conditions were different. As the requirements for change detection analysis, it is necessary to standardize the effect of atmosphere.

It assumes that the radiance in deep, clear water or shaded area in near infrared bands is zero or close to zero (Teillet and Fedosejevs 1995). All pre-processing operations were performed with Landsat OLI/TM band (SWIR) 1 band, a near infrared band that were extracted from original Landsat data sets. The Landsat Thematic Mapper (TM) and Operational Land Imager (OLI) sensors capture reflected solar energy, convert these data to radiance, then rescale this data into an 8-bit digital number (DN) with a range between 0 and 255 in Landsat-5 (TM) or into a 16-bit Digital Number (DN) with a range between 0 and 65536 in Lansat-8 (OLI). The Dark Object Subtraction (DOS) method also termed as a histogram minimum method for atmospheric correction, was applied. It is perhaps the simplest atmospheric correction approach for change detection applications (Mahiny and Turner 2007).

From conversion to TOA Reflectance Digital Number (DN) of Landsat-5 involved two steps: Equation 1 is the basic equation for converting the Digital Number (DN) to spectral radiance: The formula (1) used in this process is as follows (Markham and Barker 1986) :

$$L_\lambda = \left(\frac{LMAX - LMIN}{(QCALMAX - QCALMIN)} \right) * (DN - QCALMIN) + LMIN \quad (1)$$

Where, L_λ is the cell value as radiance, DN = Digital number, $LMIN_\lambda$ = Spectral radiance scales to QCALMIN, $LMAX_\lambda$ = Spectral radiance scales to QCALMAX, QCALMIN =The minimum quantized calibrated pixel value, QCALMAX = The maximum quantized calibrated pixel value.

Equation 2 is the basic equation for converting the spectral radiance to reflectance: The reflectance for band$_\lambda$ is computed by the following equation (Markhar and Barker 1986) :

Table 2. Accuracy assessment of vegetation maps for 1986 and 1990. Producer Accuracy (PA) and User's Accuracy (UA).

	Land cover map 1992		Land cover map 2017	
Land cover classes	PA%	UA%	PA%	UA%
Deep water bodies	100	100	100	100
Shallow water bodies	98	100	97	96
Slight water bodies	100	85	88	93
Other land cover	76	100	91	90
Sparsely vegetated area	97	100	98	95
Aggregate vegetated area	100	99	100	98
Overall accuracy%	92.23		93.1	
Kappa coefficient%	0.85		0.84	

$$\rho_\lambda = \frac{\pi . L_\lambda . d^2}{ESUN_\lambda . \cos\theta} \qquad (2)$$

ρ_λ = Unit less plantary reflectance, L_λ= Spectral radiance (from earlier step), d = Earth-Sun distance in astronomical units, $ESUN_\lambda$ = Mean solar exoatmospheric irradiances, θ_s = Solar zenith angle.

Where, L_λ is at satellite spectral radiance which is the outgoing radiation energy of the band observed at the top of atmosphere by the satellite (in this lab, we use the results calculated from step 3), d is the Earth-Sun distance in astronomical units, $ESUN_\lambda$ is mean solar exoatmospheric irradiances for the band$_\lambda$ and cosθ is the cosine of the solar incident angle. Supposing a horizontal land surface is flat, the cosine of solar incidence angle (cosθ) can be calculated from the Sun Elevation cos (90-Sun Elevation). Since the inverse of d^2 (which is $1/d^2$) in equation 3 is equivalent to inverse squared relative distance Earth-Sun, dr, the equation 3 can be rewritten as :

$$\rho_\lambda = \frac{\pi . L_\lambda}{ESUN_\lambda . \cos\theta . d_r} \qquad (3)$$

The annual averaged value of d_r is 1.0 and it ranges from about 0.97 to 1.03. You can find a real number for a special date (such as the 189 day: July 8 for this image used is 1.0167).

From Conversion to TOA Reflectance Digital Number (DN) of Landsat-8: OLI band data can also be converted to TOA planetary reflectance using reflectance-rescaling coefficients provided in the product metadata file (MTL file). The following equation is used to convert DN values to TOA reflectance for OLI data as follows (USGS 2014) :

$$\rho\lambda' = M_\rho Qcal + A\rho \qquad (4)$$

Where, M_ρ = Band-specific multiplicative rescaling factor from the metadata, A_ρ = Band-specific additive rescaling factor from the metadata, Q_{cal} = Quantized and calibrated standard product pixel values (DN), $\rho\lambda'$ = TOA planetary reflectance, without correction for solar angle. Note that ρλ' does not contain a correction for the sun angle. TOA reflectance with a correction for the the sun angle is then:

$$\rho\lambda = \frac{\rho\lambda'}{\cos(\theta_{sz})} = \frac{\rho\lambda'}{\sin(\theta_{SE})} \qquad (5)$$

Where, $\rho\lambda$ = TOA planetary reflectance, θ_{SE} = Local sun elevation angle. The scene center sun elevation angle in degrees is provided in the metadata, θ_{SZ} = Local solar zenith angle ; $\theta_{SZ} = 90^o - \theta_{SE}$.

For more accurate reflectance calculations, per pixel solar angles could be used instead of the scene center solar angle, but per pixel solar zenith angles are not currently provided with the Landsat-8 products.

NDWI and DNDWI calculation

The Normalized Difference Water Index (NDWI) is a remote sensing derived index estimating the leaf water content at canopy level. The NDWI is a remote sensing based indicator sensitive to the change in the water content (Wang et al. 2006). The NDWI, which is also called the leaf area water-absent index, could be an alternative for optical remote sensing to map flooded areas. It is possible since this index estimates the water content within vegetation (Gao 1996). NDWI is computed using the Near Infrared band (NIR) and

Table 3. Comparison land cover and post-classification between Landsat-8/OLI and Landsat-5/TM.

Classify area	Landsat-5 (TM) 1992		Land cover change		Landsat-8 (OLI) 2017	
	Sum	%	Sum	%	Sum	%
Deep water bodies	229	0.30%	281	+0.5	510	0.80%
Shallow water bodies	445	0.70%	434	+0.6	879	1.30%
Slight water bodies	3567	5.30%	– 593	– 0.9	2974	4.40%
Other land cover	48943	72.80%	3664	+5.4	52607	78.20%
Sparsely vegetated area	12081	18.00%	– 4302	– 6.4	7779	11.60%
Aggregate vegetated area	1991	3.00%	516	+0.7	2507	3.70%

the Short Wave Infrared band (SWIR 1) reflectances:

NDWI = (NIR–SWIR1) / NIR+SWIR1
Where, NIR = band (4), SWIR1 = band (5) in Landsat-5 (TM).
Where, NIR = BAND (5), SWIR1 = band (6) in Landsat-8 (OLI).

The NDWI product is dimensionless and varies between –1 to +1, depending on the leaf water content but also on the vegetation type and cover (Fig. 2). High values of NDWI correspond to high vegetation water content and to high vegetation fraction cover. Low NDWI values correspond to low vegetation water content and low vegetation fraction cover. In period of water stress, NDWI will decrease.

The post-classification method, this technique compares and computes NDWI values between images acquired on two different dates. In order to apply NDWI image differencing, the individual NDWI image of each date was generated with a range of values from. Histogram equalization enhancement was used to modify these values so that all values occurred with equal probability to range 0–255 for TM images and 0–65536 for OLI images.

This step was followed by creating NDWI difference image (DNDWI) through the subtraction of the NDWI image of one date from that on another date (Dai et al. 2010). In this study, the NDWI 1992 image was subtracted from the NDWI 2017 image as shown in the equation (7) :

$$DNDWI = NDWI\ (2017) – NDWI\ (1992) \quad (7)$$

To identify the changed areas in a different date image, a threshold technique based on differencing image histogram was selected. In this method, the significant changes were found in the tails of the histogram distribution while pixels showing no significant change had a tendency to be clustered around the means. The first step was to select the threshold, where zero is considered non-change area while values bigger or smaller than zero are considered as area of change. Finally, a change / no change map was created between 1992–2017.

Classification and accuracy assessment

In the present study, Landsat data of both dates were independently classified based on the NDWI values range from –1 to +1. The vegetation, water, cloud and snow reflect more in the near infrared band than they do in the Short Wavelength Infrared band and therefore, they have positive NDWI values, whereas, bare soil and rock have a negative NDWI value. Healthy green vegetation, on the other hand, has stronger near infrared reflectance thereby providing NDWI values close to +1. Based on this information, the two-date NDWI images were classified into 6 classes by using the NDWI threshold ranges technique or tolls in ENVI 5.3 software for preparing the region of interest. The result of Landsat-8 (OLI) images indicates that sparse vegetation NDWI values fall between 0.1 and 0.2 ; while dense or aggregate vegetation NDWI values range from 0.2 to 1. Similarly, NDWI values less than 0.1 represent water body and areas without vegetation cover.

The result of Landsat-5 (TM) images indicates that sparse vegetation NDWI values fall between 0.07 and 0.17 ; while dense or aggregate vegetation NDWI values range from 0.17 to 1. Similarly, NDWI values less than 0.07 represent water body and areas without vegetation cover. Thereafter, the region interest was selected and the maximum likelihood supervised classification algorithm was applied to generate land

cover for the two dates.

Results and Discussion

NDWI images results

The result of this process was a gray scale NDWI images representing the amount of water and vegetation present at each time. Examining a grayscale of the NDWI for each successive year was a visually simplistic way to analyze the progression of vegetation and water body area over the 26 year period.

In the first two images in Figs. 3 and 4, areas with healthy and dense vegetation are white while areas that are gray (little or sparsely vegetation area),and areas where no vegetation exists are black. The while area which represents vegetated areas and typical water has stronger near infrared reflectance. This means that most of the visible light (Short Wavelength Infrared) was used for product biomass thereby producing NDWI values ranging between 0.04 and 1. This represents regions plants with good condition, high leaf biomass, canopy closure and vegetation with high chlorophyll content (Landsat 8 2015, Tollefson 2013, Yang et al. 2015). Conversely negative NDWI values were recorded in a dark area. This is because of the fact that features reflect more in the visible band (Short Wavelength Infrared) than they do in the near infrared band, indicating regions of low vegetation and bare soil and rock (Knight and Kvaran 2014). To indicate subtler details, the gray scale NDWI results both images reclassified to 6 colored areas. The green color use to represent plants with good condition, high leaf biomass, canopy closure and vegetation with high chlorophyll content. This area involves aggregate and sparsely vegetated regions. The blue color use to represent rivers, lake, pond and other typical water bodies area. This area represents deep, Shallow or Slight Water bodies regions. The brown color use to representation of other land cover. This area includes bare soil and rock.

DNDWI results

After performing a differential analysis on the 2 NDWI results, the differences between the vegetated areas and unvegetated areas can be clearly seen in Fig. 5. In the DNDWI image Fig. 5 regions that have experienced changes are assigned in 5 class, while regions with little or on changes are shown in colored area. Likewise, dark blue areas are regions that have increase depth or dense of water body and light blue areas are regions that have decrease depth or dense of water body. Brown area are regions that have no change land cover. Dark green areas are regions that changes to aggregate of vegetation area and light green areas are regions that changes to sparse vegetated area.

Land cover maps and accuracy assessment

The NDWI values were divided into six main classes: Deep water bodies, Shallow water bodies, Slight water bodies, aggregate vegetated area, sparsely vegetated area and other land cover the classification maps were generated for two time as shown in Fig. 5. These maps are not very useful without quantitative statements about their accuracy. The accuracy assessment process was done using confuse matrix on the land cover maps which is tabulated in Table 2. It is found that, the overall accuracy and the kappa coefficient obtained using maximum likelihood classifier for 1992 are 92.23% and 0.85, while in the year 2017, 93.1% and 0.84 were obtained as shown in Table 2. In addition, the users accuracies for both time for all classes exceeded 84% and 92% respectively. Furthermore, the producers accuracy (2017) exceeded 87% of all the classes.This implies that the classification was done with the highest accuracy using the maximum likelihood classifier.

Land cover change patterns

The individual class areas and change statistics from post-classification technique for the 2 time are summarized in Table 2. The last two columns in that table show the total area and percentage change in area for each land cover type from 1992 to 2017. The results show that in 1992, the water bodies class was 4241 km^2, sparse veg 12081 km^2 aggregate veg 1991 km^2 and non-veg about 48943 km^2 respectively. By 2017, the water bodies class was 4363 km^2, sparse veg 7779 km^2, aggregate veg 2507 km^2 and non-veg about 52607 km^2 respectively.

From Table 3 and Fig. 5, it can be observed that there is a drastic decrease in the sparse vegetation shows a decrease of 4302 km^2 (6.4%). In contrast, the aggregate vegetated area was increased about 516 km^2 (0.7%). The highest increase occurring in no vegetation class (Other land cover) of 3664 km^2 (5.4%), the Deep water bodies and Shallow water bodies were increase 281 km^2 (0.5%) and 434 km^2 (0.6%) respectively, in contrast, the was decreased about 593 km^2 (0.9%). This means that most of the green land was changed to bare land or no vegetation area.

Conclusion

Generally speaking, the research results show that, the field area or planted areas are at risk of losing vegetation. Vegetation area is the first effectible about climate change condition in recent years annual rainfall of this area (Karun basin) was decrease that this condition cause to decrease sparsely vegetated area and Slight water bodies. Although Deep water bodies and Shallow water bodies have increased over the studied period. But the increase in unions is abnormal and not due to increased atmospheric precipitation in attention to performance several irrigation projects, water structures, water transfer lines and minimum 3 big dames in this basin its normally that Deep water bodies and aggregate vegetated area was increased. Also, the results of this study may indicate a decrease in the surface water source as well as a decrease in natural plant tissue during the study period. This phenomenon is due to the development of agricultural sector and the reduction of surface water resources in the Karun basin.

References

Al-doski JB, Mansor SH, Mohd Shaf HZ (2013) NDVI differencing and post-classification to detect veg changes in Halabja City, Iraq. J Appl Geol and Geophysics (IOSR-JAGG) 1 (2) : 01—10.

Anonymous (2012) USGS/EROS Find Data / Products and Data Available / TM.

Campbell JB (2002) Introduction to Remote Sensing. Guilford Press.

Ceccato P, Flasse S, Gregoire JM (2002) Designing a spectral index to estimate vegetation water content from remote sensing data : Part 2. Validation and applications. Remote Sens Environ 82 : 198—207.

Ceccato P, Flasse S, Tarantola S, Jacquemond S, Gregoire JM (2001) Detecting vegetation water content using reflectance in the optical domain. Remote Sens Environ 77 : 22—33.

Chen QL, Zhang YZ, Ekroos A, Hallikainen M (2004) The role of remote sensing technology in the EU Water Framework directive (WFD). Environ Sci Policy 7 : 267—276.

Dai Xiao-ai, Yang Wu-nian, Tang Chuan (2010) Land use and Land Cover Change Analysis using Satellite Remote Sensing and GIS, Geoscience and Remote Sensing (IITA-GRS), 2010 Second IITA International Conference on, 2010.

Du ZQ, Li WB, Zhou DB, Tian LQ, Ling F, Wang HL, Gui YM, Sun BY (2014) Analysis of Landsat-8 (OLI) imagery for land surface water mapping. Remote Sens Lett 5 : 672—681.

Feng L, Hu CM, Chen XL, Cai XB, Tian LQ, Gan WX (2012) Assessment of inundation changes of Poyang Lake using MODIS observations between 2000 and 2010. Remote Sens Environ 121 : 80—92.

Gao BC (1996) NDWI–A normalized difference water index for remote sensing of vegetation liquid water from space. Remote Sens Environ 58 (3) : 257—266.

Gu Y, Brown JF, Verdin JP, Wardlow (2007) A five year analysis of MODIS NDVI and NDWI for grassland drought assessment over the central great plains of the United States. Geophysical Res Letters, pp 34.

Hu C, Muller-Karger FE, Andrefouet S, Carder KL (2001) Atmospheric correction and cross-calibration of Landsat-7/ETM+imagery over aquatic environments: A multiplat form approach using Sea WiFS/MODIS. Remote Sens Environ 78 : 99—107.

Huang C, Chen Y, Wu JP (2014) Mapping spatio-temporal flood inundation dynamics at large river basin scale using time-series flow data and MODIS imagery. Int J Appl Earth Obs Geoinf 26 : 350—362.

Hui FM, Xu B, Huang HB, Yu Q, Gong P (2008) Modelling spatial-temporal change of Poyang Lake using multitemporal Landsat imagery. Int J Remote Sens 29 : 5767—5784.

Khuzestan Water and Power Authority (2010) Study and Executive Projects of Irrigation and Drainage Networks. Water Department. Khuzestan Water and Power Authority. Retrieved 2010-03-15.

Knight EJ, Kvaran G (2014) Landsat-8 operational land imager design, characterization and performance. Remote Sens 6 : 10286—10305.

Landsat-8 (L8) (2015) Data Handbook. Available online:http://landsat.usgs.gov/documents/ Landsat-8 Data Users Handbook.pdf(accessed on 17 June 2015).

Li WB, Du ZQ, Ling F, Zhou DB, Wang HL, Gui YM, Sun BY, Zhang XMA (2013) Comparison of land surface water mapping using the normalized difference water index from TM, ETM plus and ALI. Remote Sens 5 : 5530—5549.

Li W, Qin Y, Sun Y, Huang H, Ling F, Tian L, Ding Y (2016) Estimating the relationship between dam water level and surface water area for the Danjiangkou Reservoir using Landsat remote sensing images. Remote Sens Lett 7 : 121—130.

Mahiny AS, Turner BJ (2007) A comparison of four common atmospheric correction methods, photogramm. Engg Remote Sens 73 : 361.

Markham and Barker (1986) Landsat-7 Science User Data Handbook Chap 11, 2002.

Markham B, Knight EJ, Canova B, Donley E, Kvaran G, Lee K, Irons JR (2012) The Landsat data continuity mission operational land imager (OLI) sensor. In Proc the IEEE Int Geosci and Remote Sens Symp 2012 (IGARSS 2012), Munich, Germany, 22—27 July 2012 ,pp 6995—6998.

Markham B, Storey J, Morfitt R (2015) Landsat-8 sensor characterization and calibration. Remote Sens 7 : 2279—2282.

McFeeters SK (1996) The use of the normalized difference water index (NDWI) in the delineation of open water features. Int J Remote Sens 17 : 1425—1432.

Pahlevan N, Lee Z, Wei J, Schaaf CB, Schott JR, Berk A (2014) On-orbit radiometric characterization of OLI (Landsat-8) for applications in aquatic remote sensing. Remote Sens Environ 154 : 272—284.

Paolini L, Grings F, Sobrino J, Jiménez Muñoz JC, Karszenbaum H (2006) Radiometric correction effects in Landsat multi–date/multi-sensor change detection studies. Int J Remote Sens 27 : 685—704.

Papa F, Prigent C, Rossow WB (2008) Monitoring flood and discharge variations in the large siberian rivers from a multi-satellite technique. Surv Geophys 29 : 297—317.

Richards JA (2012) Remote Sensing Digital Image Analysis. Springer.

Richards JA, Jia X (2006) Remote Sensing Digital Image Analysis : An Introduction. Springer Verlag.

Rokni K, Ahmad A, Selamat A, Hazini S (2014) Water feature extraction and change detection using multitemporal Landsat imagery. Remote Sens 6 : 4173—4189.

Ryu JH, Won JS, Min KD (2002) Waterline extraction from Landsat TM data in a tidal flat : A case study in Gomso Bay, Korea. Remote Sens Environ 83 : 442—456.

Singh KV, Setia R, Sahoo S, Prasad A, Pateriya B (2015) Evaluation of NDWI and MNDWI for assessment of waterlogging by integrating digital elevation model and groundwater level. Geocarto Int 30 : 650—661.

Sivanpillai R, Miller SN (2010) Improvements in mapping water bodies using ASTER data. Ecol Inform 5 : 73—78.

Teillet P, Fedosejevs G (1995) On the dark target approach to atmospheric correction of remotely sensed data. Canadian J Remote Sens 21 : 374—387.

Thome KJ, Biggar SF, Wisniewski W (2003) Cross comparison of EO-1 sensors and other Earth resources sensors to Landsat-7 ETM + using Railroad Valley Playa. IEEE Trans Geosci Remote Sens 41 : 1180—1188.

Thorne K, Markharn B, Barker PS, Bigger S (1997) Radiometric calibration of Landsat. Photogramm. Engg Remote Sens 63 : 853—858.

Tollefson J (2013) Landsat-8 to the rescue. Nature 494 : 13—14.

Tucker CJ (1980) Remote sensing of leaf water content in the near infrared. Remote Sens Environ 10 : 23—32.

USGS (2014) Using the USGS Landsat-8 Product, Available online : http://landsat.usgs.gov/Landsat8_Using_Product.php (accessed on 24 November 2014).

USGS (2015) LDCM CAL/VAL Algorithm Description Document. Available online:http://landsat.usgs. gov/documents/LDCM_CVT_ADD.pdf (accessed on 17 June 2015). Remote Sens 7:10785.

Vorosmarty CJ, Sharma KP, Fekete BM, Copeland AH, Holden J, Marble J, Lough JA (1997) The storage and aging of continental runoff in large reservoir systems of the world. AMBIO 26 : 210—219.

Wang C, Lu ZH, Haithcoat TL (2006) Using Landsat images to detect oak decline in the Mark TWAIN National Forest, Ozark Highlands. For Ecol Manage 240 : 70—78.

Work EA, Gilmer DS (1976) Utilization of satellite data for inventorying prairie ponds and lakes. Photogramm. Engg Remote Sens 42 : 685—694.

Xu HQ (2006) Modification of normalized difference water index (NDWI) to enhance open water features in remotely sensed imagery. Int J Remote Sens 27 : 3025—3033.

Yang A et al. (2015) Cross-Calibration of GF-1/WFV over a Desert Site Using Landsat-8/OLI Imagery and ZY-3/TLC Data. Remote Sens 7 : 10763—10787.

Zhong B, Zhang Y, Du T, Yang A, Lv W, Liu Q (2014) Cross-calibration of HJ-1/CCD over a desert site using Landsat ETM+imagery and ASTER GDEM product. IEEE Trans Geosci Remote Sens 52 : 7247—7263.